The Astrophysical Journal, 582:17–29, 2003 January 1

LENSING AND THE CENTERS OF DISTANT EARLY-TYPE GALAXIES

Charles R. Keeton[1]
Astronomy and Astrophysics Department, University of Chicago, 5640 South Ellis Avenue, Chicago, IL 60637
Received 2002 May 22; accepted 2002 September 3

ABSTRACT

Gravitational lensing provides a unique probe of the inner 10–1000 pc of distant galaxies ($z \sim 0.2$–1). Theoretical studies have predicted that each strong lens system should have a faint image near the center of the lens galaxy, which should, in principle, be visible in radio lenses but has never been detected. We study the predicted "core" images using models derived from the stellar distributions in nearby early-type galaxies. We find that realistic lens galaxies produce a remarkably wide range of core images, with magnifications spanning some 6 orders of magnitude. More concentrated galaxies produce fainter core images, although not with any model-independent relation between the galaxy properties and the core images. Some real galaxies have diffuse cores that should yield bright core images (magnification $\mu_{\rm core} \gtrsim 0.1$), but more common are galaxies that yield faint core images ($\mu_{\rm core} \lesssim 0.001$). Thus, stellar mass distributions alone are probably concentrated enough to explain the lack of observed core images. Observational sensitivity may need to improve by an order of magnitude before detections of core images become common. Two-image lenses should tend to have brighter core images than four-image lenses, so they will be the better targets for finding core images and exploiting these tools for studying the central mass distributions of distant galaxies.

Subject headings: galaxies: elliptical and lenticular, cD — galaxies: nuclei — galaxies: structure — gravitational lensing

1. INTRODUCTION

Galaxy centers are interesting places to study dynamics and galaxy formation. Their short crossing times make them sensitive to dynamical processes such as relaxation and binary black hole heating (e.g., Ebisuzaki, Makino & Okumura 1991; Milosavljevic & Merritt 2001). Their deep potential wells collect remnants of the galaxy formation process such as the cores of accreted galaxies (e.g., de Zeeuw & Franx 1991; Barnes & Hernquist 1992). Their dark matter content provides clues to the interaction between baryons and dark matter by adiabatic compression during galaxy formation (e.g., Blumenthal et al. 1986) and may even reveal properties of the dark matter particle such as cross sections for self-interactions (e.g., Spergel & Steinhardt 2000).

Nearby galaxy centers can be studied directly with high spatial resolution observations. *Hubble Space Telescope* (*HST*) imaging of early-type galaxies shows that, contrary to theoretical expectations (e.g., Tremaine 1997), the luminosity profiles diverge at small radii (e.g., Faber et al. 1997; Ravindranath et al. 2001; Rest et al. 2001). The profiles seem to fall into two classes: "core" galaxies have a distinct transition between a steep outer profile and a shallow inner core that has $I \propto R^{-\gamma}$ with $\gamma \lesssim 0.3$, while "power-law" galaxies show no such break and have steep central cusps with $\gamma \gtrsim 0.5$. Interestingly, the global properties of the galaxies seem to correlate well with the centers. Core galaxies tend to be luminous, slowly rotating systems with boxy or elliptical isophotes, while power-law galaxies tend to be faint, rapidly rotating systems with disky isophotes. Although the division may not be as sharp as originally thought (see Ravindranath et al. 2001; Rest et al. 2001), it still puts strong constraints on the formation process. In hierarchical merging scenarios, simple models cannot easily explain why the large galaxies are so much less dense than their small progenitors (see § 7 of Faber et al. 1997 and references therein), and some additional process such as heating by binary black holes may be required (e.g., Milosavljevic & Merritt 2001; Milosavljevic et al. 2002).

For distant galaxies, we cannot directly resolve 10–100 pc scales, but we can instead turn to a unique indirect probe offered by gravitational lensing. Lens theory predicts that if the central mass distribution is shallower than $\rho \propto r^{-2}$, then any multiply imaged gravitational lens must have an odd number of images (Burke 1981; Schneider, Ehlers & Falco 1992). Standard image configurations[2] have two or four bright images lying $\sim$3–10 kpc from the center of the lens galaxy, with the remaining image just 10–100 pc from the center and at least 1 or 2 orders of magnitude fainter than the others. Because the core image is very sensitive to the central surface density of the lens galaxy, with a higher density corresponding to a fainter image, it offers a unique way to constrain the density on scales that cannot be directly resolved. This probe of galaxy centers can in principle be applied to all lens galaxies, which now number more than 60 and are predominantly early-type galaxies spanning the redshift range $z \sim 0.3$–1 (e.g., Kochanek et al. 2000). It is conceptually equivalent to using radial arcs to constrain the central profiles of lensing clusters (e.g., Mellier, Fort, & Kneib 1993; Smail et al. 1996; Molikawa & Hattori 2001; Oguri, Taruya, & Suto 2001).

The best observational data on core images come from radio lenses, because the lack of radio emission from most

[1] Hubble Fellow.

[2] The rare exceptions are a configuration where the source lies in a naked cusp and produces just three images, and configurations where the image multiplicity is larger than 4 because of the presence of multiple lens galaxies. These exceptions apply to no more than three of the more than 60 lenses currently known: B1359+154 (Rusin et al. 2001), perhaps PMN J0134−0931 (Winn et al. 2002a; Hall et al. 2002), and perhaps APM 08279+5255 (Lewis et al. 2002).

lens galaxies enables sensitive searches for core images. The Cosmic Lens All-Sky Survey found 22 radio lenses but no core images, based on radio maps where the dynamic range is typically several tens to several hundreds but reaches 1200 for B1030+074 and 2000 for B0218+357 (Rusin & Ma 2001; Norbury et al. 2002). Several other radio lenses have candidate core images (MG 1131+0456, Chen & Hewitt 1993; PMN J1632−0033, Winn et al. 2002b), although the hypothesis that the central radio flux originates in the lens galaxy cannot be ruled out. At optical and near-infrared wavelengths, APM 08279+5255 has an odd number of images (Ibata et al. 1999; Egami et al. 2000), but its interpretation is not clear. The third image may be a core image, in which case it indicates a large low-density core in the lens galaxy (Ibata et al. 1999; Egami et al. 2000; Muñoz, Kochanek, & Keeton 2001), or it may be a case of a "naked cusp" image configuration, in which case it contains no information about the center of the lens galaxy (Lewis et al. 2002). No other optical core images have been seen, although the searches are of course hindered by light from the lens galaxies.

The apparent discrepancy between data and theory provides the opportunity to learn about the centers of distant galaxies. Motivated by both theoretical expectations (see Tremaine 1997) and ease of use, many analyses have assumed models with a finite density core and obtained limits on lens galaxy core radii (e.g., Narayan, Blandford, & Natyananda 1984; Narasimha, Subramanian, & Chitre 1986; Blandford & Kochanek 1987; Hinshaw & Krauss 1987; Narayan & Schneider 1990; Wallington & Narayan 1993; Kochanek 1996; Evans & Hunter 2002). Rusin & Ma (2001) instead used power-law models and obtained a lower limit on the power-law index, $\gamma > 0.8$ at 90% confidence for a surface density $\Sigma \propto R^{-\gamma}$. The question remained, however, whether these two classes of models were realistic enough to provide robust, model-independent conclusions about lens galaxy centers. Muñoz et al. (2001) introduced double power-law models where the core region is allowed to have a power-law cusp whose index is independent of the density profile at large radii. They found that the lack of a core image in B1933+503 robustly implies $\gamma \gtrsim 0.6$ for that one galaxy. Keeton (2001) studied core images statistically using models with cuspy stellar components, treated as generalized Hernquist (1990) models, embedded in dark matter halos. He found that the models were inconsistent with the data, perhaps because generalized Hernquist models may not accurately represent the stellar components of galaxies on 10–100 pc scales.

The goal of this paper is to reconsider the core image problem using more realistic models derived from nearby galaxies and, more generally, to discuss using core images as tools for studying the centers of distant ($z \sim 0.3$–1) galaxies. Nearby early-type galaxies have surface brightnesses that can be modeled as a "Nuker" law (Lauer et al. 1995; Byun et al. 1996), and in § 2 we discuss lensing by such galaxies. In § 3 we consider in a general way what physical properties of lens galaxies determine core images properties, or conversely what we can learn about lens galaxies by studying core images. In § 4 we study in detail the core images predicted for a sample of realistic lens galaxies. Finally, in § 5 we offer a summary and conclusions. We assume the popular ΛCDM cosmology with matter density $\Omega_M = 0.3$, cosmological constant $\Omega_\Lambda = 0.7$, and Hubble constant $H_0 = 75$ km s^{-1} Mpc^{-1}.

2. NUKER-LAW LENSES

The lensing properties of a galaxy with projected mass density Σ are given by the lensing potential ϕ that satisfies the two-dimensional Poisson equation $\nabla^2\phi = 2\Sigma/\Sigma_{\rm cr}$. Here $\Sigma_{\rm cr} = (c^2 D_{os})/(4\pi G D_{ol} D_{os})$ is the critical surface density for lensing, where D_{ol}, D_{os}, and D_{ls} are angular diameter distances between the observer ("o"), the lens ("l"), and the source ("s"). We consider a fiducial lensing situation with a lens galaxy at redshift $z_l = 0.5$ and a source at redshift $z_s = 2$, which yields a critical density of $\Sigma_{\rm cr} = 2230\ M_\odot\ {\rm pc}^{-2}$ for our adopted ΛCDM cosmology. The lensing deflection is given by $\alpha = \nabla\phi$, and the magnification depends on the second derivatives of ϕ. See Schneider et al. (1992) for a full discussion of lens theory.

Because lensing selects galaxies by mass, the sample of observed lens galaxies is dominated by early-type galaxies. In many nearby early-type galaxies the surface brightness distribution is well described by a Nuker law (Lauer et al. 1995; Byun et al. 1996),

$$I(R) = 2^{(\beta-\gamma)/\alpha} I_b \left(\frac{R}{r_b}\right)^{-\gamma} \left[1 + \left(\frac{R}{r_b}\right)^{\alpha}\right]^{(\gamma-\beta)/\alpha}, \quad (1)$$

where γ and β are the inner and outer power-law indices, respectively, r_b is the radius where the break in the power law occurs, α gives the sharpness of the break, and I_b is the surface brightness at the break radius. If the luminosity distribution has circular symmetry and the mass-to-light ratio is Υ, the lensing deflection is

$$\alpha_{\rm gal}(R) = \frac{2^{1+(\beta-\gamma)/\alpha}}{2-\gamma}\,\kappa_b r_b \left(\frac{R}{r_b}\right)^{1-\gamma} \times {}_2F_1\left[\frac{2-\gamma}{\alpha}, \frac{\beta-\gamma}{\alpha}, 1+\frac{2-\gamma}{\alpha}, -\left(\frac{R}{r_b}\right)^{\alpha}\right], \quad (2)$$

where $\kappa_b = \Upsilon I_b/\Sigma_{\rm cr}$ is the surface mass density at the break radius in units of the critical density for lensing, and ${}_2F_1$ is the hypergeometric function. If the stellar distribution has ellipsoidal symmetry, the lensing deflection must be computed numerically using the formalism given by, e.g., Schramm (1990).

Most galaxies contain central supermassive black holes (e.g., Magorrian et al. 1998), so we consider adding them to the model. The deflection from a black hole is $\alpha_{\rm bh}(R) = R_{\rm E}^2/R$, where the black hole's Einstein radius is (in angular units)

$$R_{\rm E} = \left(\frac{4GM_{\rm bh}}{c^2}\frac{D_{ls}}{D_{ol}D_{os}}\right)^{1/2}. \quad (3)$$

We normalize the black holes using the observed correlation between the black hole mass $M_{\rm bh}$ and the velocity dispersion σ of the parent galaxy (Gebhardt et al. 2000; Merritt & Ferrarese 2001). The net deflection is simply the sum of the deflections from the Nuker component and the black hole.

As an example, consider the nearby galaxy NGC 4486, which has Nuker-law parameters $\alpha = 2.82$, $\beta = 1.39$, and $\gamma = 0.25$ and is a fairly typical (albeit massive) example of the early-type galaxies in the sample studied by Faber et al. (1997). Imagine a lens galaxy obtained by moving NGC 4486 to a typical lens redshift $z_l = 0.5$. The deflection profile $\alpha(R)$ for the resulting lens is shown in Figure 1. The asymptotic behavior is $\alpha(R) \propto R^{1-\gamma}$ for $R \ll r_b$ (if there is no black

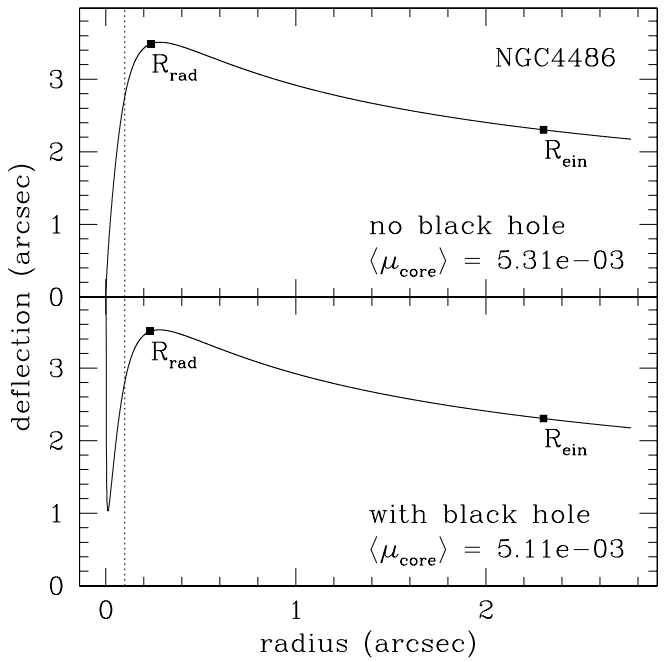

FIG. 1.—Deflection profile for a mock lens galaxy obtained by taking the nearby galaxy NGC 4486 and moving it to redshift $z_l = 0.5$. The vertical dotted line indicates the Nuker break radius r_b. The filled squares mark the critical radii R_E and R_{rad}. The top panel shows the result for the Nuker galaxy alone, while the bottom panel adds a central black hole normalized by the M_{bh}-σ relation from Gebhardt et al. (2000). The mean core image magnification $\langle\mu_{core}\rangle$ is computed with the method presented in § 3.

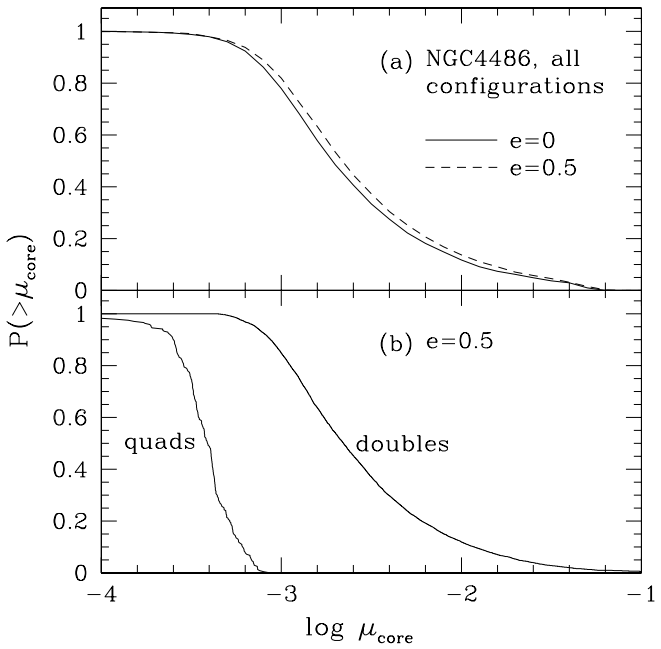

FIG. 2.—Cumulative distributions of magnification factors for the core images predicted by the NGC 4486 mock lens galaxy. (*a*) Total distributions plotted for a circular (*solid line*) or flattened (*dashed line*) lens galaxy. (*b*) Distributions plotted separately for lenses with two or four bright images (doubles or quads), for a lens galaxy with ellipticity $e = 0.5$. There is more statistical uncertainty in the curve for quads than for doubles, because of the 7917 random source positions we examined, only 238 of them corresponded to quads.

hole), and $\alpha(R) \propto R^{1-\beta}$ for $R \gg r_b$. Typical galaxies have $\gamma < 1$ and $\beta > 1$, so the deflection is zero at the origin, rises to some finite peak, then slowly declines. There are two important radii corresponding to the "critical curves," or curves along which the lensing magnification is infinite. The tangential critical curve lies at the Einstein radius R_E, which is the solution to $\alpha(R_E) = R_E$. The radial critical curve lies at the radius R_{rad} which is the solution to $d\alpha/dR = 1$. The radial critical curve maps to a caustic at

$$u_{max} = \alpha(R_{rad}) - R_{rad} \ . \quad (4)$$

This caustic bounds the multiply imaged region; sources with $u < u_{max}$ are multiply imaged, while sources with $u > u_{max}$ are not. The core images are always contained in the region bounded by the radial critical curve. The radii R_E and R_{rad} are marked in Figure 1.

If the galaxy has a steep central cusp with $\gamma > 1$, the deflection diverges at the origin and is a monotonically decreasing function of radius. In this case, the radial critical curve does not exist, and the lens never produces a core image. If the galaxy contains a central black hole, the black hole causes the deflection to diverge at the origin and suppresses some of the core images (Mao, Witt, & Koopmans 2001). However, the black hole changes the deflection only at very small radii, so it has little effect on the critical radii R_E and R_{rad} or on the mean core image magnification $\langle\mu_{core}\rangle$ (see Fig. 1). Adding a dark matter halo to the lens galaxy would raise the outer deflection profile and make it approximately flat, but it would have little effect on the central deflection profile that determines the properties of the core images unless it were much more centrally concentrated than the light.

To characterize the core images expected in this lens, we study the core image magnification distribution. The distribution can be computed fairly rapidly using inverse ray shooting (e.g., Kayser, Refsdal, & Stabell 1986; Wambsganss 1997). Figure 2*a* shows the distribution for circular and flattened lens galaxies. The distribution is broad, spanning more than 2 orders of magnitude, with a median value $\mu_{core} = 0.0019$ and a mean value $\langle\mu_{core}\rangle = 0.0053$ for the circular case. Making the galaxy flattened shifts the magnification distribution to higher values; but even for ellipticity $e = 0.5$ the shift is only 0.05 dex, so the core image magnification distribution is largely insensitive to ellipticity in the lens galaxy. (We would see more of an effect if we described core images by their flux ratio relative to the bright images, μ_{core}/μ_{bright}, because μ_{bright} is quite sensitive to ellipticity.)

Ellipticity is important in one respect. If the lens galaxy is nonspherical, some source positions correspond to lenses with two bright images (doubles), while others correspond to lenses with four bright images (quads; see, e.g., Schneider et al. 1992). Figure 2*b* shows the core image magnification distributions for quads and doubles separately. Because the sources lie farther from the origin for doubles than for quads, and the core image magnification increases with distance from the origin, doubles tend to have larger core image magnifications than quads. The quantitative details depend on the ellipticity, on any external tidal perturbation (shear) that may affect the lens, and on the stellar profile of the galaxy, but the general result is robust: quads to tend have smaller μ_{core} than doubles.

The ellipticity effect combines with an observational selection effect. Quads generally have larger total magnifications than doubles, so the sources in quads tend to be

intrinsically fainter than the sources in doubles. Together, their fainter sources and smaller core image magnifications suggest that quads will tend to have fainter core images than doubles. The lack of detected core images in quads should therefore be less surprising than in doubles. Conversely, doubles should be better systems than quads for searching for core images.

Thus, while ellipticity in the lens galaxy is important in understanding differences between quads and doubles, it is not very important in the overall distribution of core image magnifications. In the remainder of the paper we therefore neglect ellipticity and use circular lens galaxies.

3. WHAT DO CORE IMAGES PROBE?

In order to derive meaningful conclusions from observational constraints on core images, it is important to understand how core images depend on the physical properties of lens galaxies. (Merely understanding the parameter dependencies in parametric lens models does not allow strong physical conclusions.) Although the full distributions of core images predicted for a particular lens galaxy must be computed numerically, the mean magnification $\langle \mu_{\rm core} \rangle$ can be studied analytically. Moreover, in § 4 we argue that this quantity is actually a good way to characterize the distribution. Hence, in this section we study $\langle \mu_{\rm core} \rangle$ in general terms.

Formally, we have

$$\langle \mu_{\rm core} \rangle = \frac{\int_{\rm mult} \mu_{\rm core}(\boldsymbol{u})\, d\boldsymbol{u}}{\int_{\rm mult} d\boldsymbol{u}} , \tag{5}$$

$$= \frac{\int_{\rm core} d\boldsymbol{x}}{\int_{\rm mult} d\boldsymbol{u}} . \tag{6}$$

The first line is simply the definition of the average, where the integral extends over the multiply imaged region of the source plane. In the second line, the integral in the numerator extends over the core region in the image plane, defined to be the region within the radial critical curve; this equality holds because $\mu_{\rm core} = |\partial \boldsymbol{x}/\partial \boldsymbol{u}|$ is the Jacobian of the transformation between the source and image planes. In other words, equation (6) says that the mean core image magnification is equal to the area within the radial critical curve divided by the lensing cross section (the area of the multiply imaged region in the source plane). For circularly symmetric lenses,

$$\langle \mu_{\rm core} \rangle = (R_{\rm rad}/u_{\rm max})^2 . \tag{7}$$

For noncircular lenses, Figure 2 suggests that this is still a good approximation, because the $\mu_{\rm core}$ distribution is not terribly sensitive to ellipticity. These relations were first given by Keeton (2001).

Now we focus on circularly symmetric lenses. Given the definition of $u_{\rm max}$ from equation (4), we can write equation (7) as

$$\langle \mu_{\rm core} \rangle = [\alpha(R_{\rm rad})/R_{\rm rad} - 1]^{-2} , \tag{8}$$

$$= \left(\langle \kappa \rangle_{R_{\rm rad}} - 1 \right)^{-2} , \tag{9}$$

where $\langle \kappa \rangle_R$ is the mean surface density within radius R, in units of the critical density for lensing. The second equality holds because, by the definition of the deflection,

$$\frac{\alpha(R)}{R} = \frac{2}{R^2} \int_0^R \xi \kappa(\xi)\, d\xi = \langle \kappa \rangle_R . \tag{10}$$

Alternatively, returning to equation (8) and using the identities

$$\frac{\alpha(R)}{R} + \frac{d\alpha}{dR} = 2\kappa(R) , \tag{11}$$

$$\left. \frac{d\alpha}{dR} \right|_{R_{\rm rad}} = 1 , \tag{12}$$

we obtain

$$\langle \mu_{\rm core} \rangle = \tfrac{1}{4} [\kappa(R_{\rm rad}) - 1]^{-2} . \tag{13}$$

Equations (9) and (13) indicate that the mean core image magnification is given very simply from either the surface mass density at the radial critical curve $R_{\rm rad}$ or the mean surface mass density within $R_{\rm rad}$.

What remains is to understand what physical properties of the galaxy determine the radial critical curve $R_{\rm rad}$. Equating equations (9) and (13), we find that $R_{\rm rad}$ is the solution to

$$2\kappa(R_{\rm rad}) = \langle \kappa \rangle_{R_{\rm rad}} + 1 . \tag{14}$$

This relation implies that the radial critical curve is related to the concentration of the galaxy's (projected) mass distribution. We expect $\kappa(R)$ to be a decreasing function, so $\langle \kappa \rangle_R \geq \kappa(R)$ for all R. If $\kappa(R)$ is steep, the mass is concentrated and $\langle \kappa \rangle$ is large so we must go to large κ (small R) to satisfy equation (14); equation (13) then implies faint core images.[3] Conversely, if $\kappa(R)$ is shallow, then equation (14) is satisfied at smaller κ (larger R), and the core images are brighter.

These results can be demonstrated with two simple examples. First, consider a softened isothermal sphere with surface mass density $\kappa(R) = (b/2)(s^2 + R^2)^{-1/2}$, where s is a core radius and b is a scale radius that equals the Einstein radius in the case $s = 0$. The critical radii and mean core image magnification are

$$R_{\rm E} = [b(b - 2s)]^{1/2} , \tag{15}$$

$$R_{\rm rad} = \tfrac{1}{2} \zeta (\xi + \zeta)^{1/2} (\xi - 3\zeta)^{1/2} , \tag{16}$$

$$u_{\rm max} = \tfrac{1}{4} (\xi + \zeta)^{1/2} (\xi - 3\zeta)^{3/2} , \tag{17}$$

$$\langle \mu_{\rm core} \rangle = \left(\frac{2\zeta}{\xi - 3\zeta} \right)^2 , \tag{18}$$

where $\xi = (4b + s)^{1/2}$ and $\zeta = s^{1/2}$. Decreasing the core radius reduces $\langle \mu_{\rm core} \rangle$, with $\langle \mu_{\rm core} \rangle \approx s/b$ for $s \ll b$. Second, consider a power-law density $\rho \propto r^{-\gamma}$ or $\kappa \propto R^{1-\gamma}$, with $\gamma > 1$ to ensure that $\kappa(R)$ is a decreasing function. The crit-

[3] This result also explains how adding a central black hole affects the mean core image magnification. The black hole suppresses some core images, reducing $\langle \mu_{\rm core} \rangle$ (Mao et al. 2001). In the language of our analysis, the black hole increases $\langle \kappa \rangle_R$ without changing $\kappa(R)$, so we must move to larger κ (smaller R) to keep eq. (14) satisfied.

ical radii and mean core image magnification are

$$R_{\rm rad} = R_{\rm E}(2-\gamma)^{1/(\gamma-1)}\ , \tag{19}$$

$$u_{\rm max} = R_{\rm E}(\gamma-1)(2-\gamma)^{(2-\gamma)/(\gamma-1)}\ , \tag{20}$$

$$\langle\mu_{\rm core}\rangle = \left(\frac{2-\gamma}{\gamma-1}\right)^2 . \tag{21}$$

Increasing γ (making the profile steeper) decreases $\langle\mu_{\rm core}\rangle$. These expressions are valid only for $1 < \gamma < 2$, because for $\gamma > 2$ the density profile is so steep that the radial critical curve does not exist and the model does not produce core images. Previous studies used specific models like these to understand the inverse relation between the brightness of core images and the concentration of the lens galaxy, but equations (13) and (14) now give it in a general, model-independent form.

4. CORE IMAGES IN REALISTIC GALAXIES

4.1. *The Sample*

To understand core images in realistic galaxies, we study models constructed from a sample of observed galaxies. This approach ensures that we examine the region of parameter space occupied by real systems. We seek galaxies with well-resolved luminosity profiles, plus measured velocity dispersions as mass indicators. Faber et al. (1997), Carollo et al. (1997), Carollo & Stiavelli (1998), and Ravindranath (2001) have published samples of nearby early-type galaxies observed with high-resolution *HST* imaging at optical or near-infrared wavelengths.[4] Together the samples comprise 73 distinct galaxies with both Nuker-law fits and velocity dispersions, which are summarized in Table 1. The different samples use different passbands: *V* for the Faber sample, *H* for the Ravindranath sample, and *V* and *I* for the Carollo sample. However, we can check for wavelength dependence and other systematic effects because some of the galaxies appear in more than one sample: six galaxies in both the Faber and Ravindranath samples, five galaxies in both the Faber and Carollo samples, six galaxies in both the Ravindranath and Carollo samples, and 10 galaxies with multiple passbands in the Carollo sample. (No galaxies appear in all three samples.)

We use this sample to construct mock lens galaxies by moving each galaxy to a typical lens redshift $z_l = 0.5$ and assuming a typical source redshift $z_s = 2$. Following Faber et al. (1997), we compute the mass-to-light ratio for each galaxy using a spherical and isotropic dynamical model. Faber et al. (1997) give mass-to-light ratios for their sample, providing a check for our calculations. We then compute the lensing properties of the mock lens galaxies, which are summarized in Table 1.

As discussed in § 2 we focus on circularly symmetric galaxies because ellipticity has little effect on the overall distribution of core image magnifications. We consider only the Nuker components of the galaxies, neglecting any nuclear components that may be indicated by fits to the surface brightness distribution. This is a conservative approach to the core image problem, because any additional mass concentration would decrease the predicted core image magnifications and bring the models closer to agreement with the data. We also neglect dark matter halos. Dark matter does not appear to be dynamically important in the inner 5–10 kpc of elliptical galaxies (e.g., Gerhard et al. 2001). While it is important for lensing (because lensing depends on the projected mass; e.g., Koopmans & Treu 2002), dark matter would have little effect on the projected mass distributions on the $\lesssim$200 pc scales important for core images unless it were substantially more concentrated than the light.

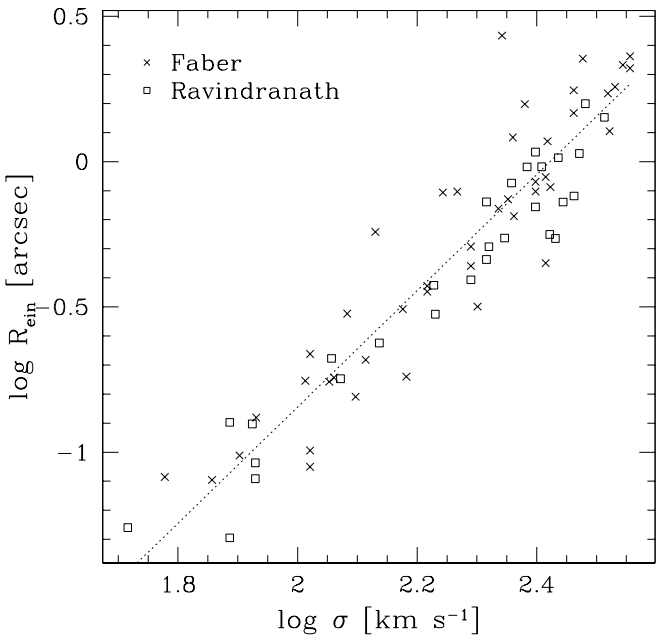

FIG. 3.—Relation between the velocity dispersion σ and Einstein radius $R_{\rm E}$ for the mock lens galaxies. Crosses and squares indicate galaxies in the Faber and Ravindranath samples, respectively. The dotted line shows the relation $R_{\rm E} \propto \sigma^2$; the fitted zero point is −4.84 (in log units), compared with a predicted value of −4.74 for comparable SISs.

We can check that our mock lenses are reasonable in several ways. First, we compute the Einstein radius for each galaxy and compare it to the velocity dispersion in Figure 3; this tests whether the lensing and dynamical masses are consistent. For comparison, a simple singular isothermal sphere (SIS) lens has the scaling $R_{\rm E} \propto \sigma^2$, with a zero point of −4.74 (in log units) for $z_l = 0.5$ and $z_s = 2$ in our adopted ΛCDM cosmology (see Schneider et al. 1992). The mock galaxies are consistent with this scaling and a fitted zero point of −4.84, although with a scatter of 0.16 dex. The fact that the mock galaxies lie, on average, 0.1 dex below the expected SIS relation may be related to our neglect of dark matter halos. Still, the dynamical and lensing properties are related in a sensible way suggesting that the mock lens galaxies are not unreasonable.

As a second check, we consider the galaxies that appear in more than one of the original samples. For example, for each galaxy that was observed and modeled by both Faber et al. (1997) and Ravindranath et al. (2001), we compute the lensing properties using both models and compare them. In this way we test whether the use of different modeling techniques and different passbands affects our lensing results. Figure 4 compares the Einstein radii and mean core image magnifications for all of the duplicate galaxies. There is fair agreement in the Einstein radii, although with some scatter because different studies find somewhat different values of

[4] Rest et al. (2001) give a similar sample but without velocity dispersions.

TABLE 1

GALAXY SAMPLE

Name (1)	D (Mpc) (2)	σ (km s^{-1}) (3)	α (4)	β (5)	γ (6)	$\log \kappa_b$ (7)	$\log r_b$ (arcsec) (8)	$\log R_{\rm E}$ (arcsec) (9)	$\log R_{\rm rad}$ (arcsec) (10)	$\log\langle\mu_{\rm core}\rangle$ (11)	$\log\langle\mu_{\rm core}\rangle$ (12)	$\log\langle\mu_{\rm core}\rangle$ (13)	Reference (14)
NGC 221	0.9	85	0.98	1.36	0.01	2.86	−4.02	−1.26	−3.17	−4.67	−6.00	−6.00	1
	0.7	77	4.66	1.26	0.50	2.56	−3.71	−1.29	−3.28	−4.74	−6.00	−5.31	2
NGC 224	0.9	220	4.72	0.87	0.12	3.25	−3.65	0.43	−0.58	−1.65	−1.66	−1.66	1
NGC 474	32.5	169	1.23	1.90	0.37	0.91	−1.39	−0.43	−1.30	−2.08	−2.10	−2.10	2
NGC 524	24.6	275	1.29	1.00	0.00	1.96	−2.21	0.29	−0.85	−2.13	−2.18	−2.21	1
	32.1	242	0.68	1.69	0.03	1.26	−1.41	−0.02	−0.98	−2.12	−2.15	−2.16	2
NGC 596	22.6	165	0.76	1.97	0.55	0.62	−1.20	−0.43	−1.44	−2.31	−2.37	−2.36	1
NGC 720	24.1	250	2.32	1.66	0.06	1.12	−1.21	−0.07	−0.90	−1.97	−1.99	−1.99	1
NGC 821	23.2	207	1.00	1.59	0.64	1.31	−1.66	−0.34	−1.60	−3.03	−3.20	−3.23	2
NGC 1023.....	10.9	217	4.72	1.18	0.78	1.52	−1.80	−0.16	−1.52	−2.99	−3.11	−3.14	1
NGC 1052.....	17.8	222	1.05	1.43	0.11	1.94	−2.22	−0.26	−1.58	−3.15	−3.28	−3.32	2
NGC 1172.....	31.8	113	1.52	1.64	1.01	0.18	−1.21	−0.76	−6.00	−6.00	−6.00	−6.00	1
NGC 1316.....	19.1	240	1.16	1.00	0.00	1.85	−2.21	0.20	−0.87	−1.96	−1.99	−2.01	1
NGC 1399.....	19.1	333	1.50	1.68	0.07	1.49	−1.33	0.10	−0.95	−2.66	−2.69	−2.72	1
NGC 1400.....	22.9	265	1.39	1.32	0.00	2.08	−2.22	−0.09	−1.49	−3.29	−3.44	−3.52	1
NGC 1426.....	22.9	150	3.62	1.35	0.85	0.89	−1.53	−0.51	−1.52	−2.25	−2.31	−2.30	1
NGC 1600.....	53.5	340	1.98	1.50	0.08	1.02	−0.88	0.26	−0.52	−1.68	−1.69	−1.70	1
NGC 1700.....	37.9	230	0.90	1.30	0.00	2.23	−2.57	−0.19	−1.62	−3.27	−3.51	−3.59	1
	54.1	230	0.46	1.65	0.01	1.80	−2.08	−0.17	−1.40	−2.80	−2.93	−2.96	3*V*
	54.1	230	0.47	1.68	0.01	1.81	−2.08	−0.19	−1.44	−2.89	−3.03	−3.07	3*I*
NGC 2636.....	35.7	85	1.84	1.14	0.04	1.41	−2.59	−0.88	−1.87	−1.97	−2.01	−1.99	1
NGC 2685.....	16.2	114	1.69	1.52	0.73	0.64	−1.48	−0.68	−1.56	−1.87	−1.90	−1.89	2
NGC 2832.....	96.2	330	1.84	1.40	0.02	1.27	−1.16	0.23	−0.68	−2.02	−2.04	−2.06	1
NGC 2841.....	14.1	229	0.93	1.02	0.01	2.35	−2.84	0.08	−1.17	−2.41	−2.53	−2.56	1
NGC 3115.....	9.0	280	1.47	1.43	0.78	1.60	−1.69	−0.13	−1.61	−3.59	−4.18	−6.00	1
	6.7	264	1.13	1.80	0.73	1.36	−1.51	−0.25	−1.65	−3.62	−4.00	−6.00	2
NGC 3377.....	10.6	152	1.92	1.33	0.29	2.53	−3.12	−0.74	−2.57	−4.48	−6.00	−6.00	1
NGC 3379.....	10.6	225	1.59	1.43	0.18	1.61	−1.84	−0.21	−1.35	−2.72	−2.78	−2.80	1
	8.1	209	1.82	1.45	0.18	1.71	−1.96	−0.29	−1.50	−2.95	−3.02	−3.03	2
NGC 3384.....	8.1	170	5.36	1.58	0.64	1.35	−1.78	−0.52	−1.61	−2.80	−2.84	−2.84	2
NGC 3599.....	21.7	80	13.01	1.66	0.79	0.50	−1.64	−1.01	−1.65	−1.34	−1.35	−1.34	1
NGC 3605.....	21.7	103	9.14	1.26	0.67	0.92	−1.82	−0.75	−1.64	−1.84	−1.86	−1.85	1
NGC 3608.....	21.7	195	1.05	1.33	0.00	1.88	−2.32	−0.29	−1.53	−2.80	−2.90	−2.91	1
	13.6	195	0.72	1.58	0.00	1.88	−2.28	−0.37	−1.63	−3.03	−3.15	−3.16	3*V*
	13.6	195	0.78	1.57	0.00	1.92	−2.32	−0.39	−1.67	−3.11	−3.25	−3.26	3*I*
NGC 3900.....	29.4	118	0.29	1.66	0.51	1.39	−2.24	−0.75	−2.37	−3.65	−6.00	−6.00	2
NGC 4026.....	17.0	195	0.88	1.50	0.68	1.51	−1.92	−0.41	−1.84	−3.41	−3.94	−4.07	2
NGC 4143.....	17.0	270	1.26	2.18	0.59	1.20	−1.35	−0.26	−1.45	−3.23	−3.35	−3.42	2
NGC 4150.....	9.7	85	1.23	1.67	0.58	1.18	−2.28	−1.09	−2.20	−2.69	−2.79	−2.74	2
NGC 4168.....	38.8	185	0.95	1.50	0.14	0.76	−1.11	−0.10	−0.82	−1.24	−1.25	−1.25	1
NGC 4239.....	16.3	60	14.53	0.96	0.65	0.39	−1.78	−1.09	−1.71	−0.75	−0.76	−0.75	1
NGC 4261.....	35.1	326	2.38	1.43	0.00	1.43	−1.32	0.15	−0.86	−2.38	−2.41	−2.44	2
NGC 4278.....	9.7	250	1.63	1.39	0.02	1.96	−2.10	−0.16	−1.50	−3.25	−3.36	−3.40	2
	9.7	250	1.45	1.32	0.00	1.98	−2.13	−0.09	−1.43	−3.12	−3.23	−3.27	3*V*
	9.7	250	1.25	1.46	0.00	1.90	−2.04	−0.15	−1.43	−3.13	−3.22	−3.25	3*I*
NGC 4291.....	29.4	278	2.07	1.48	0.02	1.89	−1.92	−0.14	−1.44	−3.28	−3.38	−3.43	2
NGC 4365.....	23.5	262	2.06	1.27	0.15	1.43	−1.51	0.07	−0.96	−2.25	−2.28	−2.30	1
	13.8	262	1.67	1.46	0.11	1.58	−1.63	−0.04	−1.15	−2.66	−2.71	−2.73	3*V*
	13.8	262	1.52	1.49	0.04	1.61	−1.67	−0.06	−1.17	−2.69	−2.73	−2.75	3*I*
NGC 4374.....	16.8	296	2.15	1.50	0.13	1.53	−1.47	0.03	−1.05	−2.66	−2.70	−2.72	2
NGC 4387.....	16.3	105	3.36	1.59	0.72	0.38	−1.24	−0.66	−1.33	−1.24	−1.26	−1.25	1
NGC 4406.....	16.8	250	3.31	1.16	0.00	1.70	−1.84	0.03	−1.19	−2.61	−2.67	−2.69	2
	13.8	250	4.13	1.05	0.04	1.80	−1.95	0.13	−1.12	−2.51	−2.58	−2.61	3*V*
	13.8	250	3.32	1.07	0.00	1.81	−1.97	0.12	−1.14	−2.55	−2.63	−2.66	3*I*
NGC 4417.....	16.8	84	0.87	1.77	0.71	0.10	−1.28	−0.90	−1.80	−1.75	−1.80	−1.78	2
NGC 4434.....	16.3	115	0.98	1.78	0.70	0.60	−1.51	−0.74	−1.77	−2.31	−2.39	−2.35	1
NGC 4458.....	16.3	105	5.26	1.43	0.49	2.02	−2.81	−0.99	−2.51	−3.87	−4.04	−3.96	1
NGC 4464.....	16.3	125	1.64	1.68	0.88	0.96	−1.81	−0.81	−2.08	−3.11	−6.00	−3.35	1
NGC 4467.....	16.3	72	7.52	2.13	0.98	0.02	−1.38	−1.10	−2.75	−3.38	−6.00	−6.00	1
NGC 4472.....	16.3	300	2.08	1.17	0.04	1.51	−1.51	0.24	−0.82	−2.21	−2.24	−2.26	1
	16.8	303	1.89	1.29	0.04	1.48	−1.42	0.20	−0.84	−2.29	−2.32	−2.34	2
NGC 4478.....	16.3	135	3.32	0.84	0.43	1.75	−2.66	−0.24	−1.17	−1.39	−1.42	−1.42	1
NGC 4486.....	16.3	360	2.82	1.39	0.25	1.32	−1.01	0.36	−0.63	−2.28	−2.29	−2.31	1

TABLE 1—*Continued*

Name (1)	D (Mpc) (2)	σ (km s^{-1}) (3)	α (4)	β (5)	γ (6)	$\log \kappa_b$ (7)	$\log r_b$ (arcsec) (8)	$\log R_{\rm E}$ (arcsec) (9)	$\log R_{\rm rad}$ (arcsec) (10)	$\log\langle\mu_{\rm core}\rangle$ (11)	$\log\langle\mu_{\rm core}\rangle$ (12)	$\log\langle\mu_{\rm core}\rangle$ (13)	Reference (14)
NGC 4486B ...	16.3	200	2.78	1.33	0.14	2.24	−2.63	−0.50	−2.10	−3.90	−4.33	−4.38	1
NGC 4551.....	16.3	121	2.94	1.23	0.80	0.54	−1.30	−0.52	−1.36	−1.56	−1.59	−1.58	1
NGC 4552.....	16.3	260	1.48	1.30	0.00	1.93	−2.08	−0.05	−1.36	−3.02	−3.12	−3.16	1
	13.8	260	2.17	1.06	0.00	2.06	−2.25	0.14	−1.23	−2.79	−2.92	−2.98	3*V*
	13.8	260	2.10	1.08	0.04	2.06	−2.23	0.12	−1.27	−2.87	−3.00	−3.06	3*I*
NGC 4564.....	16.3	165	0.25	1.90	0.05	1.61	−2.17	−0.45	−1.80	−3.02	−3.33	−3.29	1
NGC 4570.....	16.3	195	3.72	1.49	0.85	1.04	−1.44	−0.36	−1.43	−2.57	−2.65	−2.65	1
NGC 4589.....	30.0	228	1.09	1.18	0.11	1.93	−2.27	−0.07	−1.32	−2.64	−2.75	−2.77	2
	24.4	228	0.43	1.62	0.00	1.55	−1.80	−0.05	−1.12	−2.30	−2.35	−2.36	3*V*
	24.4	228	0.50	1.58	0.01	1.68	−1.95	−0.11	−1.24	−2.50	−2.58	−2.59	3*I*
NGC 4621.....	16.3	250	0.19	1.71	0.50	1.16	−1.42	−0.10	−1.90	−3.94	−6.00	−6.00	1
NGC 4636.....	16.3	210	1.64	1.33	0.13	1.14	−1.38	−0.04	−0.90	−1.77	−1.78	−1.78	1
	17.0	207	1.69	1.56	0.13	1.07	−1.30	−0.14	−0.96	−1.84	−1.85	−1.85	2
NGC 4649.....	16.3	360	2.00	1.30	0.15	1.55	−1.34	0.32	−0.79	−2.50	−2.54	−2.57	1
NGC 4697.....	11.2	175	24.86	1.04	0.74	1.27	−1.64	−0.11	−1.26	−2.24	−2.28	−2.28	1
NGC 4742.....	13.3	105	48.60	1.99	1.09	0.78	−1.83	−1.05	−6.00	−6.00	−6.00	−6.00	1
NGC 4874.....	99.5	290	2.33	1.37	0.13	0.71	−0.68	0.25	−0.39	−1.08	−1.08	−1.09	1
NGC 4889.....	99.5	350	2.61	1.35	0.05	1.06	−0.88	0.33	−0.47	−1.66	−1.68	−1.69	1
NGC 5273.....	21.3	52	7.03	1.32	0.37	0.48	−1.93	−1.26	−1.79	−0.72	−0.73	−0.73	2
NGC 5813.....	30.2	225	2.15	1.33	0.08	1.50	−1.72	−0.13	−1.19	−2.42	−2.46	−2.47	1
	21.2	225	1.77	1.41	0.03	1.57	−1.79	−0.17	−1.27	−2.58	−2.62	−2.63	3*V*
	21.2	225	1.67	1.46	0.01	1.58	−1.80	−0.20	−1.29	−2.62	−2.67	−2.68	3*I*
NGC 5838.....	28.5	290	2.57	1.87	0.93	0.83	−0.98	−0.12	−1.29	−2.97	−6.00	−6.00	2
NGC 5845.....	30.1	260	1.27	2.74	0.51	1.03	−1.27	−0.35	−1.44	−3.14	−3.23	−3.27	1
NGC 5982.....	38.7	256	1.73	1.28	0.06	1.65	−1.80	−0.02	−1.16	−2.57	−2.62	−2.65	2
	39.9	256	2.15	1.19	0.12	1.64	−1.79	0.03	−1.13	−2.50	−2.55	−2.58	3*V*
	39.9	256	2.17	1.19	0.12	1.64	−1.80	0.03	−1.13	−2.51	−2.57	−2.59	3*I*
NGC 6166.....	120.0	300	3.32	0.99	0.08	0.67	−0.68	0.35	−0.27	−0.74	−0.75	−0.76	1
NGC 6340.....	22.0	137	2.46	1.28	0.59	1.61	−2.28	−0.62	−1.91	−2.97	−3.09	−3.06	2
	18.0	137	1.73	1.24	0.72	1.38	−2.08	−0.57	−1.80	−2.70	−2.83	−2.79	4
NGC 7332.....	21.7	130	4.25	1.34	0.90	1.12	−1.88	−0.68	−1.87	−2.76	−2.93	−2.86	1
NGC 7457.....	12.3	77	2.32	1.03	0.35	1.22	−2.46	−0.90	−1.83	−1.67	−1.71	−1.69	2
NGC 7626.....	45.3	273	1.84	1.30	0.36	1.57	−1.64	0.01	−1.15	−2.65	−2.71	−2.75	2
	49.5	273	1.53	1.23	0.00	1.64	−1.77	0.08	−1.03	−2.40	−2.45	−2.47	3*V*
	49.5	273	1.29	1.27	0.00	1.65	−1.78	0.07	−1.04	−2.42	−2.47	−2.49	3*I*
NGC 7743.....	24.4	85	5.36	1.38	0.50	1.47	−2.48	−1.04	−2.19	−2.76	−2.82	−2.79	2
NGC 7768.....	110.0	290	1.92	1.21	0.00	1.39	−1.46	0.17	−0.82	−2.04	−2.07	−2.08	1

NOTE.—Col. (2): Distance (assuming $H_0 = 75$ km s^{-1} Mpc^{-1}). Col. (3): Central stellar velocity dispersion. Cols. (4)–(6): Fitted Nuker-law parameters. Cols. (7)–(10): Logarithms of the lensing strength κ_b, break radius r_b, Einstein radius $R_{\rm E}$, and radial critical radius $R_{\rm rad}$. Note that if any quantity is zero, we arbitrarily set its logarithm to −6. Col. (11): Logarithm of mean core image magnification for the Nuker-law lens. Cols. (12)–(13): Logarithm of mean core image magnification for the Nuker-law lens plus a supermassive black hole normalized by the $M_{\rm bh}$-σ correlations of Gebhardt et al. (2000) and Merritt & Ferrarese (2001), respectively.

REFERENCES.—(1) Faber et al. 1997; (2) Ravindranath et al. 2001; (3*V*, 3*I*) *V*- and *I*-band samples, respectively, from Carollo et al. 1997; (4) Carollo & Stiavelli 1998.

the outer slope β. The main outlier is NGC 524, where dust is known to affect the luminosity profile at optical wavelengths (Lauer et al. 1995; Ravindranath et al. 2001). There is good agreement in the mean core image magnification, so our conclusions about the properties of core images are not sensitive to whose data we use. For the remainder of the paper, we adopt as our main sample all of the Ravindranath galaxies plus the Faber galaxies that are not in the Ravindranath sample.

4.2. *A Plethora of Core Images*

Figure 5*a* shows the core image magnification distributions for nine of the mock lens galaxies to illustrate the range of effects. Each mock lens galaxy has a distribution of core image magnifications that spans some 2 orders of magnitude, and the complete set of mock lenses spans 6 orders of magnitude in $\mu_{\rm core}$. Realistic lens galaxies produce a remarkably wide range of core images.

Studying the full $\mu_{\rm core}$ distribution for each mock lens galaxy is impractical, so we would like to describe each galaxy by a single characteristic quantity. We propose to use the mean core image magnification $\langle\mu_{\rm core}\rangle$ as a good characteristic value, partly because this quantity is easy to compute (see § 3) and partly because Figure 5*b* suggests that it is indeed characteristic of the overall distribution. Specifically, when plotted in terms of the normalized quantity $\mu_{\rm core}/\langle\mu_{\rm core}\rangle$, the distributions for a wide range of galaxies all lie on top of each other. Although there are differences in the shapes of the distributions at the faint end, the distributions at the bright end are quite similar. Hence, we believe that $\langle\mu_{\rm core}\rangle$ is a useful characterization of the distribution of core image magnifications for a particular galaxy, especially at the bright end.

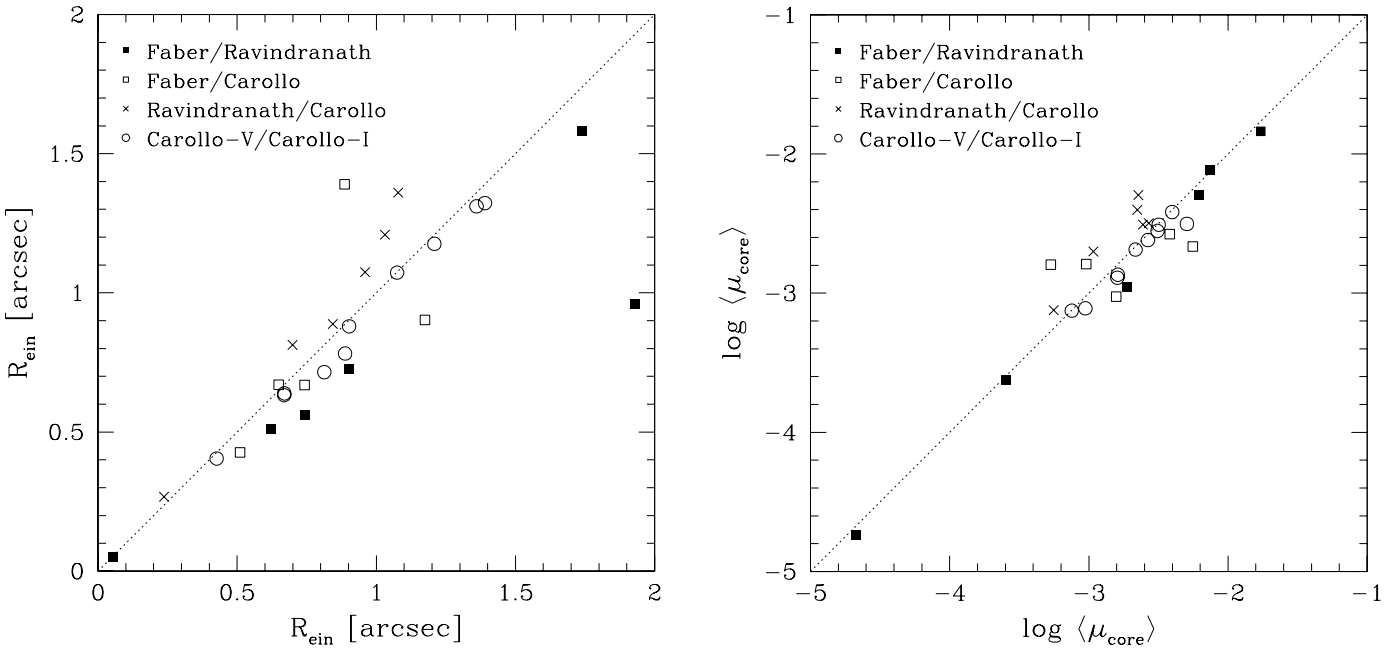

FIG. 4.—Comparison of the Einstein radii (*left*) and mean core image magnifications (*right*) for galaxies that appear in more than one of the original samples. Filled squares indicate galaxies in both the Faber and Ravindranath samples, open squares the Faber and Carollo samples, and crosses the Ravindranath and Carollo samples. Open circles indicate galaxies in both the *V*- and *I*-band Carollo samples.

Figure 6 shows a histogram of the $\langle\mu_{\rm core}\rangle$ values for the 73 mock lens galaxies. (The values are given in Table 1.) Note that the histogram is intended only to show the broad range of core image properties in our sample; it should not be interpreted as a global distribution of $\langle\mu_{\rm core}\rangle$ values, because our sample is not a statistical sample of galaxies. Still, the histogram is instructive in illustrating that the mean values $\langle\mu_{\rm core}\rangle$ span more than 4 orders of magnitude, from $\langle\mu_{\rm core}\rangle = 1.8 \times 10^{-5}$ for NGC 221 to $\langle\mu_{\rm core}\rangle = 0.19$ for NGC 5273—plus two galaxies that never produce core images (NGC 1172 and NGC 4742). Again we see the wide range of core image properties in realistic lens galaxies; some lenses should have bright, detectable core images, while others should have core images that are essentially invisible.

In principle, the central supermassive black holes that are common in galaxies can suppress core images (Mao et al. 2001), but in practice they have little effect. Table 1 gives the values for $\langle\mu_{\rm core}\rangle$ when the galaxies contain black holes normalized by the $M_{\rm bh}$-σ relations measured by Gebhardt et al. (2000) and Merritt & Ferrarese (2001). In a few cases the

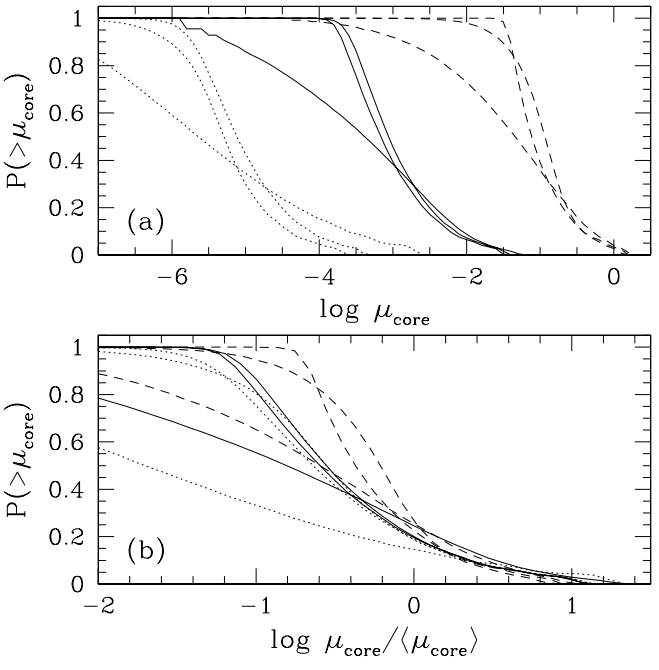

FIG. 5.—Cumulative core image magnification distributions for nine of the mock lens galaxies: the three with the lowest nonzero values for $\langle\mu_{\rm core}\rangle$ (*dotted lines*; NGC 221, NGC 3377, NGC 4621); the three with values for $\langle\mu_{\rm core}\rangle$ at the median of the sample (*solid lines*; NGC 4570, NGC 5982, NGC 4649); and the three with the largest values for $\langle\mu_{\rm core}\rangle$ (*dashed lines*; NGC 4239, NGC 6166, NGC 5273). (*a*) Distributions of the core image magnification $\mu_{\rm core}$. (*b*) Distributions of the normalized magnification $\mu_{\rm core}/\langle\mu_{\rm core}\rangle$.

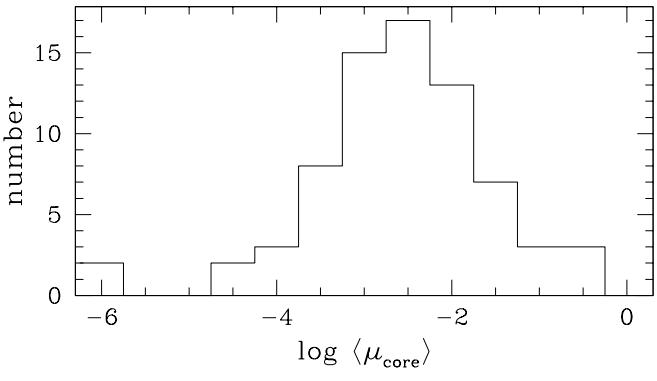

FIG. 6.—Histogram of the mean core image magnifications for the 73 mock lens galaxies. Galaxies that do not produce core images are arbitrarily placed at $\log\langle\mu_{\rm core}\rangle = -6$.

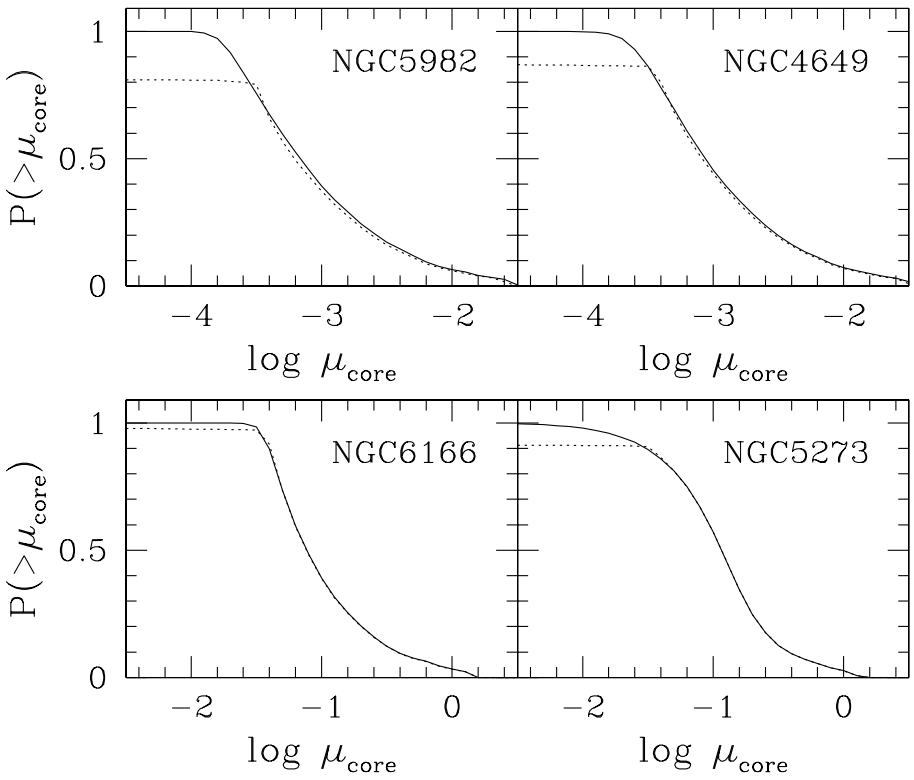

FIG. 7.—Core image magnification distributions for galaxies with (*dotted lines*) and without (*solid lines*) central supermassive black holes, for four of the galaxies from Fig. 5. Black holes can suppress core images (see Mao et al. 2001) but only at the faint end of the core image distribution.

black hole modifies the central potential enough to erase all core images (NGC 221, NGC 3115, NGC 3377, NGC 3900, NGC 4464, NGC 4467, NGC 4621, and NGC 5838). But all of these cases have $\langle \mu_{\rm core} \rangle \leq 0.001$ even without a black hole, which suggests that adding a black hole can erase all core images only if the core images are faint to begin with. In the remaining cases the black hole reduces $\langle \mu_{\rm core} \rangle$ by only about 0.1 dex. The black hole does suppress some core images, but only at the *faint* end of the distribution, as shown in Figure 7. In other words, black holes have little effect on the core images in realistic lens galaxies, especially at the bright end of the core image distribution. Therefore, black holes fail to resolve the core image paradox. These conclusions are based on local measurements of the $M_{\rm bh}$-σ relation, which may not hold at higher redshifts; but black holes would have to be substantially more massive (relative to their parent galaxies) at $z \sim 0.5$ than at $z = 0$ in order to change our conclusions. Another possibility is that binary black holes are common in galaxies at $z \sim 0.5$. In principle, binary black holes can be more effective than single black holes at suppressing core images, but for realistic binary parameters the differences are small and binary black holes do not strongly suppress core images (C. R. Keeton & H. Zhao 2003, in preparation). In the remainder of the paper we neglect black holes.

We now seek to understand the diversity of core image properties in the mock lens galaxies and to identify the galaxy properties that affect the core images. First, we examine the region of the galaxy that is probed by core images. Recall that the core images are always contained within the inner lensing critical curve, which has radius $R_{\rm rad}$ (see § 2). Figure 8 shows that the core image region has a characteristic scale ~200 pc (the median value of $R_{\rm rad}$ for the sample) and is comparable to or slightly larger than the Nuker break radius. Thus, core images probe the inner tens to hundreds of parsecs at the centers of galaxies.

Next, we consider how the mean core image magnification $\langle \mu_{\rm core} \rangle$ depends on various properties of the galaxies, as

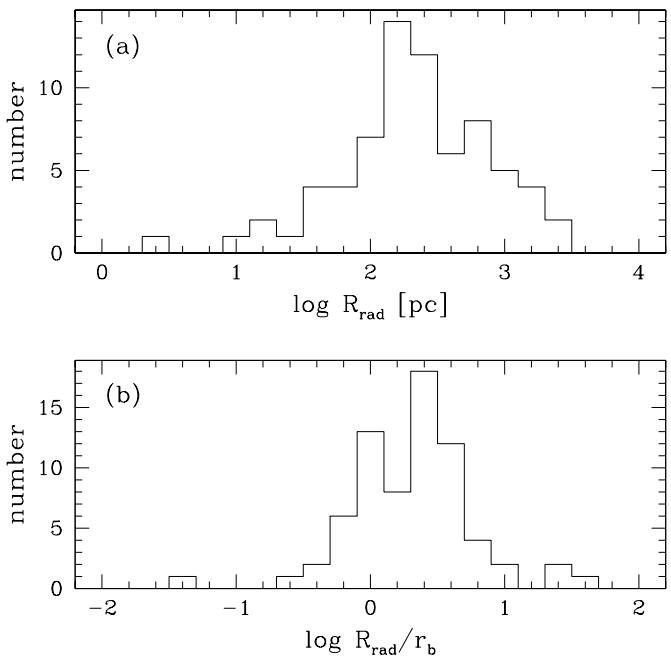

FIG. 8.—Histograms of the lensing critical radius $R_{\rm rad}$, which bounds the core image region. (*a*) The critical radius in parsecs. (*b*) The ratio of the critical radius to the Nuker break radius r_b. Galaxies that lack a critical radius $R_{\rm rad}$ are not included.

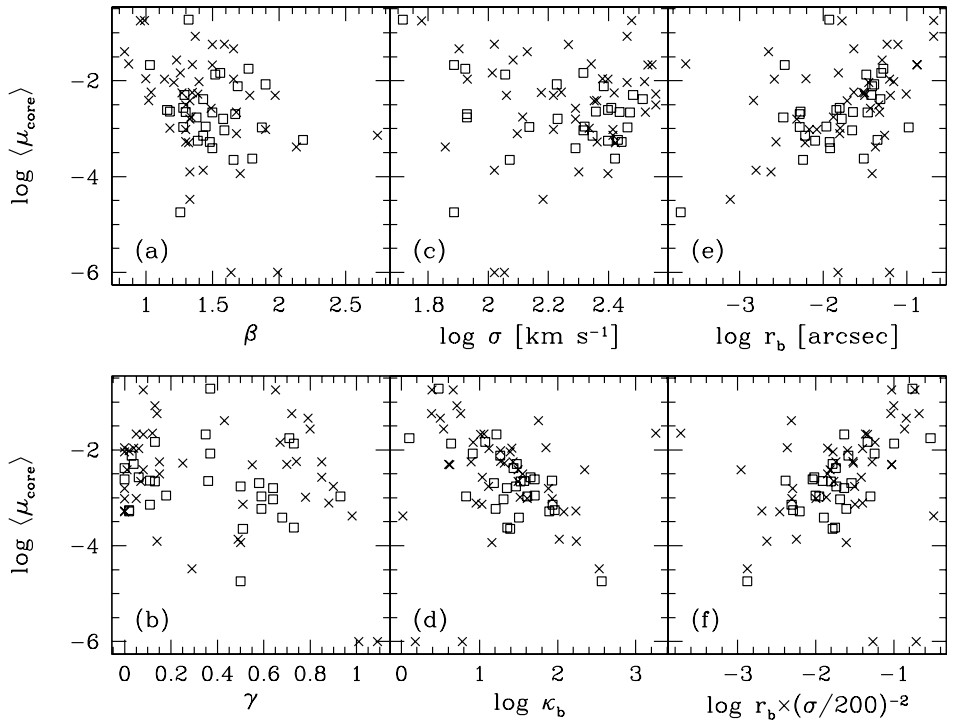

FIG. 9.—Scatter plots of the mean core image magnifications $\langle\mu_{\rm core}\rangle$ vs. various galaxy properties. Crosses and squares indicate galaxies in the Faber and Ravindranath samples, respectively. Galaxies that do not produce core images are arbitrarily placed at $\log\langle\mu_{\rm core}\rangle = -6$.

shown in Figure 9. The interesting general result is that no single property of a galaxy strongly determines its core image properties. There is no simple relation between $\langle\mu_{\rm core}\rangle$ and the outer and inner Nuker power-law indices β and γ (Figs. 9*a* and 9*b*). This result makes sense in combination with Figure 8: the lensing critical radius $R_{\rm rad}$ is often comparable to the Nuker break radius r_b, so we are in a regime where the galaxy cannot be described as a simple power law, and $\langle\mu_{\rm core}\rangle$ is not dominated by either β or γ separately. The distinction between core and power-law galaxies seen in their luminosity profiles and dynamics (Faber et al. 1997) does not appear to carry over into lensing and core images. There is likewise no simple relation between $\langle\mu_{\rm core}\rangle$ and galaxy mass (as represented by velocity dispersion; Fig. 9*c*); galaxies with a given σ have $\langle\mu_{\rm core}\rangle$ values that range over some 3 orders of magnitude or more. Dwarf galaxies are not systematically more or less likely than giant galaxies to produce bright core images.

On the basis of the arguments in § 3 we expect a connection between the core image properties and some measure of the concentration of the mass distribution. There is a trend between $\langle\mu_{\rm core}\rangle$ and the surface density at the break radius κ_b (Fig. 9*d*): galaxies with higher break densities tend to produce fainter core images. There is also a general trend between with the Nuker break radius r_b (Fig. 9*d*): galaxies with smaller break radii, and hence smaller core regions, tend to produce fainter core images. But this trend is neither strong nor tight, because by itself r_b cannot distinguish between galaxies that are large and highly concentrated and those that are less concentrated but intrinsically small. One way to remove this effect is to normalize the break radius using the Einstein radius as a measure of the global scale of the galaxy; because $R_{\rm E} \propto \sigma^2$, we actually use r_b/σ^2 (Fig. 9*f*). These three trends all indicate that there is indeed some connection between the core images and the concentration of the galaxy such that more concentrated galaxies tend to produce fainter core images. However, the trends have significant scatter and thus are not highly predictive. In other words, there does not appear to be a simple measure of a galaxy's concentration that strongly determines its core image properties.

To summarize, realistic lens galaxies have an extremely wide range of core image properties; some should have bright, detectable core images, while others should have core images that are very faint or absent altogether. A galaxy's core image properties are related to its mass concentration, but there does not appear to be any simple measure of concentration that yields a clean prediction of the core image properties. The complication is that in Nuker-law lenses the lensing critical radius $R_{\rm rad}$ tends to be comparable to the break radius r_b, which means that all of the Nuker parameters affect the core image properties. This conclusion has a somewhat surprising corollary. We might expect that the distinction between core and power-law galaxies, with their different luminosity profiles, would be obvious in their core image properties, but it is not.

4.3. *Should We See Core Images?*

We can now reevaluate the core image problem in terms of our expectations for realistic lens galaxies. Although our sample is not a proper statistical sample of galaxies, if we assume that it does at least represent the range of realistic galaxy properties, then we can consider whether the lack of observed core images is surprising or not. The main issue is to understand what types of lens galaxies produce bright core images and whether we should expect to find many lenses from such galaxies. There are three galaxies in the

sample with $\langle \mu_{\rm core} \rangle > 0.1$: two are dwarf galaxies (NGC 4239 and NGC 5273), while the third is a giant elliptical galaxy at the center of a cluster (NGC 6166). Because lensing selects galaxies by mass it tends to select against dwarf galaxies, so even if some dwarf galaxies are good at producing core images they are unlikely to produce lenses in the first place. As for NGC 6166, it is unusual for being the brightest cluster galaxy as well as the most distant (120 Mpc) and least concentrated (lowest surface brightness and largest break radius) galaxy in the Faber et al. (1997) sample. Thus, it appears to be an atypical galaxy drawn from the tail of the galaxy population. Statistically, lensing is not likely to select rare galaxies to be lens galaxies.

Lensing selection effects are important for core images in another way. Consider a set of galaxies that are similar to each other, specifically a set of galaxies with the same Einstein radius. Within this set, are galaxies that produce bright core images any more or less likely to be selected for lensing than galaxies that produce faint core images? Figure 10 shows the lensing cross section, normalized by the area within the Einstein ring, versus $\langle \mu_{\rm core} \rangle$. There is a clear decrease in the normalized cross section with increasing $\langle \mu_{\rm core} \rangle$, and it does not depend on whether magnification bias is included or omitted. The trend for the mock lens galaxies agrees well with analytic predictions for simple softened power-law lens models. Thus, at fixed Einstein radius, galaxies that produce bright core images have smaller lensing cross sections than galaxies that produce faint core images, so they are less likely to be selected for lensing. There is an intrinsic bias against lenses with bright core images.

Thus, the types of galaxies that can produce bright core images are probably not common, and they have small lensing cross sections relative to galaxies that are comparably massive but produce faint core images. The two effects combine to suggest that bright core images are not likely to be prevalent in observed lens samples.

4.4. *Comparison with Data*

The observational constraints on core images take the form of upper limits on the core image flux $f_{\rm core}$ in observed lenses. The magnification cannot be directly constrained because the intrinsic flux of the source is unknown. One way around this problem is to use the flux ratio of the core image to the brightest image, because the source flux factors out to leave $f_{\rm core}/f_{\rm bright} = \mu_{\rm core}/\mu_{\rm bright}$. This approach requires explicitly solving the lens equation to find all images and thus is valuable for applications like lens modeling where the lens equation must be solved anyway (e.g., Muñoz et al. 2001). While it can be used for statistical analyses (e.g., Rusin & Ma 2001; Keeton 2001), it eliminates technical simplifications like the ability to compute $\langle \mu_{\rm core} \rangle$ rapidly without solving the lens equation (but see Evans & Hunter 2002 for a different technical approach). It also makes the conclusions sensitive to quantities like ellipticity in the lens galaxy, because $\mu_{\rm core}$ is fairly insensitive to ellipticity but $\mu_{\rm bright}$ is not.

An alternate approach is to fit a lens model to the observed images to constrain the source flux and then combine the inferred source flux with the limits on $f_{\rm core}$ to put limits on $\mu_{\rm core}$. This approach should be robust because the model properties that determine the source flux from the observed images (the enclosed mass on 3–10 kpc scales) decouple from the properties that affect core images (the density profile on $\lesssim$200 pc scales). With this approach, Norbury et al. (2002) obtain upper limits on $\mu_{\rm core}$ for 15

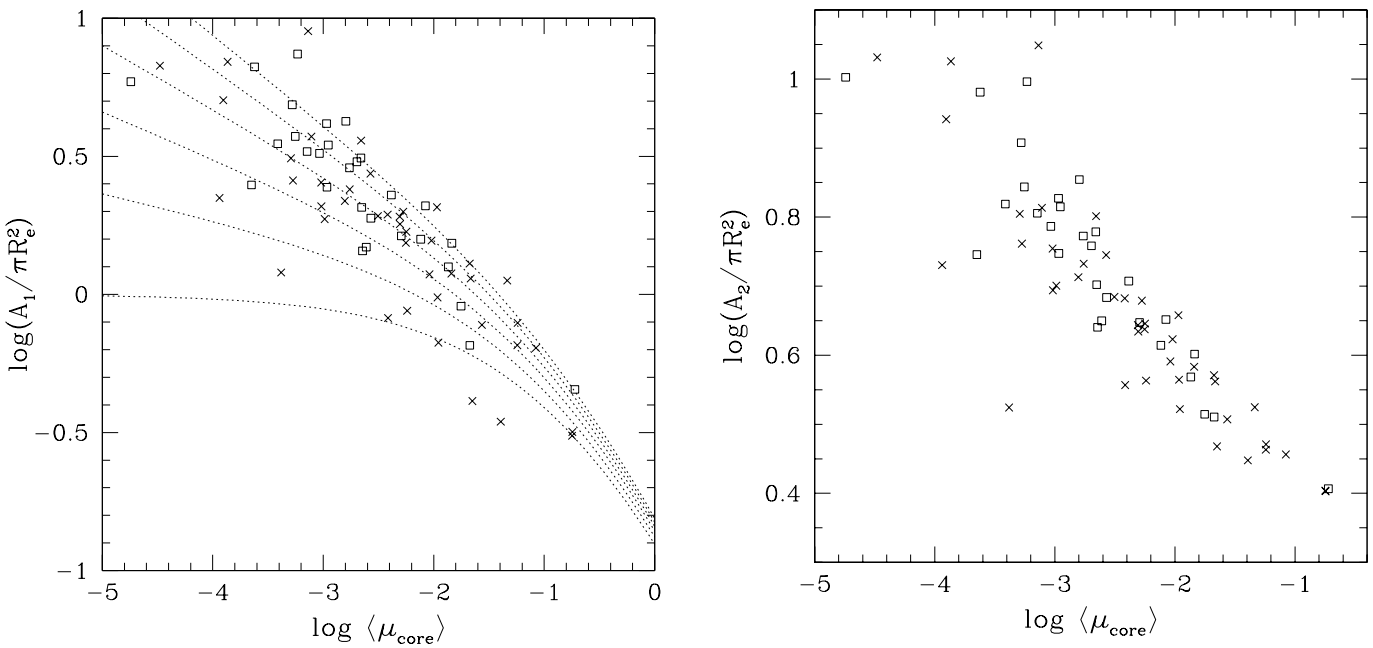

FIG. 10.—Scatter plots of the lensing cross section vs. the core image magnification. The cross sections are normalized by the area within the Einstein ring, $\pi R_{\rm E}^2$. *Left*: A_1 is the simple lensing cross section, or the area of the multiply imaged region in the source plane. The curves show results for simple softened power-law lens models $\Sigma \propto (s^2 + R^2)^{-\beta}$ with $\beta = 1.0$, 1.1, 1.2, 1.3, 1.4, and 1.5 from bottom to top. *Right*: A_2 is the lensing cross section corrected for magnification bias.

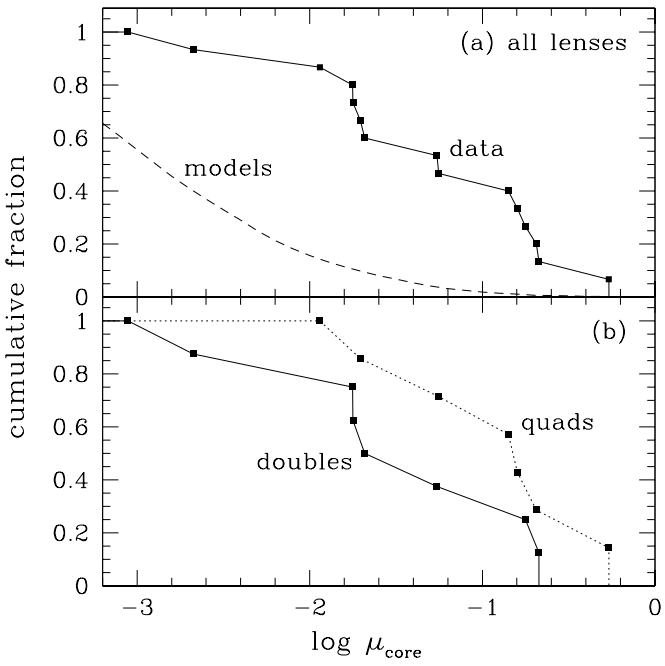

FIG. 11.—Upper limits on core image magnifications for 15 observed radio lenses (Norbury et al. 2002). The points show 5σ upper limits on $\mu_{\rm core}$. (*a*) The data for all lenses. The dashed curve shows the net $\mu_{\rm core}$ distribution predicted by a weighted sum of the model galaxies (see text). (*b*) The data for doubles and quads shown separately.

radio lenses from the Cosmic Lens All-Sky Survey, as shown in Figure 11.

For an accurate comparison, we need a prediction of the overall $\mu_{\rm core}$ distribution from the models (not merely the set of $\langle\mu_{\rm core}\rangle$ values for the sample galaxies, as in Fig. 6). A proper prediction is impossible because, again, our sample is not a statistical sample of galaxies. Nevertheless, for the sake of comparison we naïvely combine our sample by summing all of the $\mu_{\rm core}$ distributions (a few of which are shown in Fig. 5), weighting each galaxy by its lensing cross section. The result is shown as the dashed curve in Figure 11. It is interesting to see that the model predictions lie well below the limits from the data. The models do not predict that core images should be brighter than observed. In fact, they suggest that the observational sensitivity may need to improve by more than an order of magnitude before detections of core images become common. Despite concerns that the model sample is not statistically complete, we believe that the general conclusion is reliable. Galaxies that produce bright core images would have to be substantially more common in the universe than in our sample in order to make the model predictions inconsistent with the current observational data.

Evans & Hunter (2002) reach similar conclusions from an analysis of softened power-law potential models. They argue that the break radii in the galaxies observed by Faber et al. (1997) are small enough to make core images faint even if the galaxies have simple finite-density cores. Although we believe our models to be more realistic because they allow more general cores and are constructed directly from the fitted profiles, it is reassuring that the conclusions are consistent.

We previously found that Hernquist model galaxies predict core images to be more common than observed (Keeton 2001). Like a Nuker law, a Hernquist model has a steep outer profile that smoothly changes to a shallow central cusp but with a larger transition radius. Our new models should be more realistic because they are based on fits to the luminosity profiles of observed galaxies, which have small transition radii. The smaller break radii mean higher central densities and thus fainter predicted core images.

Another interesting result from the data is that the upper limits from quads are weaker than the upper limits from doubles (Fig. 11*b*). The flux limits for the various lenses are comparable, but the quads tend to have fainter sources. Combining this result with our prediction that quads will tend to have fainter core images than doubles (Fig. 2*b*), we conclude that the lack of core images in observed quad lenses is no surprise at all.

5. CONCLUSIONS

Core images in strong gravitational lens systems provide a unique probe of the centers of galaxies at redshifts $z \sim 0.2$–1. The brightnesses of core images are determined by the density profiles of galaxies inside $\lesssim 200$ pc. The lack of core images in observed lenses, especially in radio lenses, sets strong lower limits on the central densities of the lens galaxies (e.g., Wallington & Narayan 1993; Muñoz et al. 2001).

The mapping between core images and galaxy centers can be studied in two directions. In the forward problem knowledge of galaxy centers is used to make predictions about core images. On the basis of the first lens models drawn directly from the resolved stellar mass distributions of nearby early-type galaxies, we predict that real galaxies should produce a remarkably wide range of core images. Some should have bright core images (magnification $\mu_{\rm core} \gtrsim 0.1$), while many others will have core images that are faint ($\mu_{\rm core} \lesssim 0.001$) or absent altogether.

Qualitatively, more concentrated galaxies produce fainter core images. Quantitatively, however, there does not seem to be a simple predictive relation between observed galaxy properties and core images. Lensing is biased against galaxies with bright core images, because they have smaller cross sections than comparable galaxies with faint core images. Four-image lenses should tend to have fainter core images than two-image lenses, because in quads the source is always close to the center of the lens galaxy where the core image magnification is low. Supermassive black holes in the centers of galaxies can suppress faint core images, but they have little effect on bright core images or on the mean magnification.

The connection between core images and galaxy centers can also be studied in the inverse problem, where the analysis of core image data yields constraints on the centers of lens galaxies. Previous work placed limits on the core radius or on the logarithmic slope of the density (e.g., Wallington & Narayan 1993; Rusin & Ma 2001), but it was not clear how model-dependent those constraints were. We obtain a general statement of the connection between the density profile and core images: the mean core image magnification $\langle\mu_{\rm core}\rangle$ is inversely related to the density at the lensing critical radius $R_{\rm rad}$ (eq. [13]), and this critical radius is determined by the shape of the density profile (eq. [14]), with more concentrated galaxies corresponding to smaller critical radii and fainter core images. Unfortunately, neither our general formalism nor our Nuker-law lenses suggest any simple,

model-independent measure of the mass concentration that determines the core image properties. The interpretation of core image data will therefore continue to rely on detailed models of individual lenses. The model dependence can be held in check, however, by using general models like the Nuker law or the cuspy lenses introduced by Muñoz et al. (2001), as opposed to simple flat core or pure power-law models.

We conclude that in many cases the stellar mass in lens galaxies is probably concentrated enough to render core images faint (also see Evans & Hunter 2002). This is not to say that bright core images cannot exist—certainly there are realistic galaxies that can produce bright core images, and the probability that they are selected for lensing is nonzero. But the fact that core images have not yet been found (with perhaps one or two exceptions) is probably not a surprise. As the search continues, two-image lenses should be better targets than four-image lenses for revealing core images.

I am very grateful to Marijn Franx for discussions that contributed to the birth and development of this project. I also thank Martin Norbury for interesting discussions and for providing data in advance of publication. This work was supported by NASA through Hubble Fellowship grant HST-HF-01141.01-A from the Space Telescope Science Institute, which is operated by the Association of Universities for Research in Astronomy, Inc., under NASA contract NAS5-26555.

REFERENCES

Barnes, J. E., & Hernquist, L. 1992, ARA&A, 30, 705
Blandford, R. D., & Kochanek, C. S. 1987, ApJ, 321, 658
Blumenthal, G. R., Faber, S. M., Flores, R., & Primack, J. R. 1986, ApJ, 3301, 27
Burke, W. L. 1981, ApJ, 244, L1
Byun, Y.-I., et al. 1996, AJ, 111, 1889
Carollo, C. M., Franx, M., Illingworth, G. D., & Forbes, D. A. 1997, ApJ, 481, 710
Carollo, C. M., & Stiavelli, M. 1998, AJ, 115, 2306
Chen, G. H., & Hewitt, J. N. 1993, AJ, 106, 1719
de Zeeuw, T., & Franx, M. 1991, ARA&A, 29, 239
Ebisuzaki, T., Makino, J., & Okumura, S. K. 1991, Nature, 354, 212
Egami, E., Neugebauer, G., Soifer, B. T., Matthews, K., Ressler, M., Becklin, E. E., Murphy, T. W., & Dale, D. A. 2000, ApJ, 535, 561
Evans, N. W., & Hunter, C. 2002, ApJ, 575, 68
Faber, S., et al. 1997, AJ, 114, 1771
Gebhardt, K., et al. 2000, ApJ, 539, L13
Gerhard, O., Kronawitter, A., Saglia, R. P., & Bender, R. 2001, AJ, 121, 1936
Hall, P. B., Richards, G. T., York, D. G., Keeton, C. R., Bowen, D. V., Schneider, D. P., Schlegel, D. J., & Brinkmann, J. 2002, ApJ, 575, L51
Hernquist, L. 1990, ApJ, 356, 359
Hinshaw, G., & Krauss, L. M. 1987, ApJ, 320, 468
Ibata, R. A., Lewis, G. F., Irwin, M. J., Lehár, J., & Totten, E. J. 1999, AJ, 118, 1922
Kayser, R., Refsdal, S., & Stabell, R. 1986, A&A, 166, 36
Keeton, C. R. 2001, ApJ, 561, 46
Kochanek, C. S. 1996, ApJ, 466, 638
Kochanek, C. S., Falco, E. E., Impey, C. D., Lehár, J., McLeod, B. A., Rix, H.-W., Keeton, C. R., Muñoz, J. A., & Peng, C. Y. 2000, ApJ, 543, 131
Koopmans, L. V. E. , & Treu, T. 2002, ApJ, 568, L5
Lauer, T. R., et al. 1995, AJ, 110, 2622
Lewis, G., Carilli, C., Papadopoulos, P., & Ivison, R. J. 2002, MNRAS, 330, L15
Magorrian, J., et al. 1998, AJ, 115, 2285
Mao, S., Witt, H. J., & Koopmans, L. V. E. 2001, MNRAS, 323, 301
Mellier, Y., Fort, B., & Kneib, J.-P. 1993, ApJ, 407, 33
Merritt, D., & Ferrarese, L. 2001, ApJ, 547, 140
Milosavljevic, M., & Merritt, D. 2001, ApJ, 563, 34
Milosavljevic, M., Merritt, D., Rest, A., & van den Bosch, F. C. 2002, MNRAS, 331, L51
Molikawa, K., & Hattori, M. 2001, ApJ, 559, 544
Muñoz, J. A., Kochanek, C. S., & Keeton, C. R. 2001, ApJ, 558, 657
Narasimha, D., Subramanian, K., & Chitre, S. M. 1986, Nature, 321, 45
Narayan, R., Blandford, R., & Nityananda, R. 1984, Nature, 310, 112
Narayan, R., & Schneider, P. 1990, MNRAS, 243, 192
Norbury, M. A., Rusin, D., Jackson, N., Browne, I. W. A., & Wilkinson, P. N. 2002, MNRAS, submitted
Oguri, M., Taruya, A., & Suto, Y. 2001, ApJ, 559, 572
Ravindranath, S., Ho, L. C., Peng, C. Y., Filippenko, A. V., & Sargent, W. L. W. 2001, AJ, 122, 653
Rest, A., van den Bosch, F. C., Jaffe, W., Tran, H., Tsvetanov, Z., Ford, H. C., Davies, J., & Schafer, J. 2001, AJ, 121, 2431
Rusin, D., & Ma, C.-P. 2001, ApJ, 549, L33
Rusin, D., et al. 2001, ApJ, 557, 594
Schneider, P., Ehlers, J., & Falco, E. E. 1992, Gravitational Lenses (New York: Springer)
Schramm, T. 1990, A&A, 231, 19
Smail, I., Dressler, A., Kneib, J.-P., Ellis, R. S., Couch, W. J., Sharples, R. M., & Oemler, A. 1996, ApJ, 469, 508
Spergel, D. N., & Steinhardt, P. J. 2000, Phys. Rev. Lett., 84, 3760
Tremaine, S. 1997, in Unsolved Problems in Astrophysics, ed. J. N. Bahcall & J. P. Ostriker (Princeton: Princeton Univ. Press), 137
Wallington, S., & Narayan, R. 1993, ApJ, 403, 517
Wambsganss, J. 1997, MNRAS, 284, 172
Winn, J. N., Lovell, J. E. J., Chen, H.-W., Fletcher, A. B., Hewitt, J. N., Patnaik, A. R., & Schechter, P. L. 2002a, ApJ, 564, 143
Winn, J. N., Morgan, N. D., Hewitt, J. N., Kochanek, C. S., Lovell, J. E. J., Patnaik, A. R., Pindor, B., Schechter, P. L., & Schommer, R. A. 2002b, AJ, 123, 10